# SANDIA REPORT

SAND2018-9478
Unlimited Release
Printed August 2018

# The use of atmospheric prediction models to invert infrasound for linear-equivalent time domain moment tensors: Source Physics Experiment, Phase 1

Christian Poppeliers, Katherine Anderson Aur, and Leiph Preston

Prepared by
Sandia National Laboratories
Albuquerque, New Mexico 87185 and Livermore, California 94550

Sandia National Laboratories is a multimission laboratory managed and operated by National Technology and Engineering Solutions of Sandia, LLC., a wholly owned subsidiary of Honeywell International, Inc., for the U.S. Department of Energy's National Nuclear Security Administration under contract DE-NA0003525.



Sandia National Laboratories

Issued by Sandia National Laboratories, operated for the United States Department of Energy by National Technology and Engineering Solutions of Sandia, LLC.



SAND2018-9478
Unlimited Release
Printed August 2018

# The use of atmospheric prediction models to invert infrasound for linear-equivalent time domain moment tensors: Source Physics Experiment, Phase 1

Christian Poppeliers, Katherine Anderson Aur, and Leiph Preston
Geophysics Department
Sandia National Laboratories
P.O. Box 5800
Albuquerque, NM 87185-9999
cpoppel@sandia.gov

**Abstract**

We invert far field infrasound data for the equivalent seismo-acoustic time domain moment tensor to assess the effects of variable atmospheric models as well as to quantify the relative contributions of two presumed source phenomena. The infrasound data was produced by a series of underground chemical explosions that were conducted during the Source Physics Experiment, (SPE) which was originally designed to study explosion-generated seismo-acoustic signal phenomena. The goal of the work presented herein is two-fold: the first goal is to investigate the sensitivity of the estimated time domain moment tensors to variability of the estimated atmospheric model. The second goal is to determine the relative contribution of two possible source mechanisms to the observed infrasonic wave field. Rather than using actual atmospheric observations to estimate the necessary atmospheric Green's functions, we build a series of atmospheric models that rely on publicly available, regional atmospheric observations and the assumption that the acoustic energy results from a linear combination of an underground isotropic explosion and surface spall. The atmospheric observations are summarized and interpolated onto a 3D grid to produce a model of sound speed at the time of the experiment. For each of four SPE acoustic datasets that we invert, we produced a suite of three atmospheric models, based on ten years of regional meteorological observations: an average model, which averages the atmospheric conditions for ten years prior to each SPE event,

as well as two extrema models. We find that the inversion yields relatively repeatable results for the estimated spall source. Conversely, the estimated isotropic explosion source is highly variable. This suggests that the majority of the observed acoustic energy is produced by the spall source and/or our modeling of the elastic energy propagation, and it's subsequent conversion to acoustic energy via linear elastic-to-acoustic coupling at the free surface, is too simplistic.

# Acknowledgment

The authors acknowledge the National Nuclear Security Administration, Defense Nuclear Nonproliferation Research and Development (DNN R&D), and the Source Physics Experiment (SPE) working group, a multi-institutional and interdisciplinary group of scientists and engineers. Sandia National Laboratories is a multimission laboratory managed and operated by National Technology and Engineering Solutions of Sandia LLC, a wholly owned subsidiary of Honeywell International Inc. for the U.S. Department of Energy's National Nuclear Security Administration under contract DE-NA0003525.

# Contents

# List of Figures

# List of Tables

# Chapter 1

# Introduction

Fully and partially contained single-charge underground chemical explosions can be used as surrogates for underground nuclear explosions to study explosion source physics (e.g. Stump *et. al*, 1999; Arrowsmith *et al.*, 2010; Ford *et al.*, 2014; Gitterman *et al.*, 1998, Patton *et al.*, 2005). In addition to seismic energy, a significant amount of infrasonic energy can be generated, which can aid in the detection, discrimination, and forensic analysis of buried explosions (e.g. Che *et al.*, 2014). The two primary mechanisms of generating infrasonic acoustic energy include linear seismic-to-acoustic coupling at the Earth's free surface and the near source effects of non-linear ground deformation (spall). A given explosion will excite these two mechanisms to differing degrees depending on the yield, scaled depth-of-burial, and geologic structure (Ford *et al.*, 2010). Therefore by inverting infrasonic data for the individual terms of an effective source it's possible, in principle, to constrain the relative contribution of each mechanism for a given explosion event. However, inverting infrasonic data relies on an reasonably accurate physical model that accounts for the relevant wave phenomena. Factors that effect acoustic wave velocity include, but are not limited to, wind velocity, temperature, pressure, and humidity, all of which can vary as a function of spatial location. Furthermore, the atmosphere is dynamic, meaning that the source-to-receiver acoustic arrival times can vary as a function of time.

In this report, we describe the results of inverting infrasonic data for the linear-equivalent time domain moment tensor. In so doing, we have two primary goals: 1) to investigate the sensitivity of the estimated time domain source time functions to variability/uncertainty in the atmospheric model and 2) to determine the relative contribution of each potential source mechanism to the observed infrasonic data. For this work, the source receiver distance ranged from one to five kilometers, which allows us to investigate the effects of the atmospheric models at a local scale. Rather than using actual atmospheric observations, we attempt to predict the physical state of the atmosphere for a specified time and location using publicly available historic atmospheric data. These data are then used to construct estimates of the atmospheric state at the time and location of the SPE events, which we then use to estimate the necessary Green's functions. The point is to evaluate whether we can robustly invert the data using Green's functions produced from publicly available data rather than actual atmospheric measurement at the time and location of the experiment, which may not always be available in operational settings. The data that we invert was generated by four controlled underground chemical explosions conducted as part of the Source Physics Experiment, Phase 1 (SPE) which were conducted in Nevada, U.S.A. (Snelson *et al*, 2013). For the next stage of this work we will use locally obtained atmospheric measurements, taken at the time of the SPE chemical explosions, to construct atmospheric models which we will subsequently

use to invert the data to compare to the results that we present here. The results of this future work will be described in a forthcoming SAND report.

We invert four infrasonic datasets, one for each SPE event. However, we invert each dataset three times, one for each of three atmospheric Green's functions estimates. To estimate the Green's functions, we use a finite difference scheme to simulate the propagation of an acoustic wave field, where the initial condition is a band-limited delta function that corresponds to our assumed source type. The finite difference scheme requires the use of an atmospheric model that takes into account various phenomena that control the acoustic wave propagation velocity. To construct these models, we use snap shots of the atmosphere for a specified day-of-year (DOY) and time of day (TOD) for ten years preceding the date of a given SPE event. This atmospheric data is averaged and combined with topography to produce a predicted average atmospheric model for the DOY/TOD that corresponds to the given SPE event. We then produce two additional atmospheric models for each SPE event: these additional models correspond to extrema states (e.g. coldest and windiest DOY/TOD, warmest and calmest DOY/TOD). We find that the when using these different models to invert each SPE data set, the spall term of the time-domain moment tensor is stable and repeatable, albeit with slight differences in timing and wave form shape that likely is a result of the differences in the atmospheric models. Conversely, the estimated explosion term of the time domain moment tensor is highly erratic, with virtually no repeatability. This suggests that the contribution of the explosion term in the source is negligible and/or that our model of acoustic propagation does not properly account for the seismic energy.

# Chapter 2

# Method

The Source Physics Experiment is a long-term research and development effort designed to improve nuclear nonproliferation verification capabilities, particularly with respect to detection, discrimination, and yield determination associated with small-yield nuclear explosions. The SPE Phase 1 consisted of a series of controlled and well-recorded chemical explosions at the Nevada National Security Site (NNSS), where factors such as depth-of-burial, explosive yield, and geology were controlled and/or known. We focus our work here on the infrasonic data that was produced from four explosions. The data was collected on a series of surface-mounted acoustic sensors (Figure 2.1) where the attempt was made to isolate the sensors from the explosion-generated seismic arrivals. All of the explosions occurred in the same borehole, located in granite bedrock, where the depth and yield of the explosive varied for each event (Table 2.1). Although six experiments were conducted over a span of approximately five years, we only analyze the data from four of the experiments due to acceptable signal-to-noise conditions. Furthermore, we only analyze the data collected at sensors located more than one kilometer from the source, thereby ensuring that seismic energy didn't superpose the acoustic energy. The acoustic sensors were arranged in arrays of four instruments and were distributed along two azimuthal directions: a single array of instruments was located approximately one kilometer due east from the explosion site and the other three arrays were located due south of the explosion site at approximate distances of one, two, and five kilometers.

### 2.0.1 Moment Tensor Inversion

We use a frequency domain inversion technique to invert for time dependent source moment tensors of the four explosions (Stump and Johnson, 1977; Yang and Bonner, 2009). The frequency domain approach allows us to resolve the relative contribution of the two presumed source mechanisms as well as their time evolution. The model assumes that the far-field data can be predicted by the convolution of an equivalent point seismo-acoustic source with the Green's function describing the atmosphere's impulse response:

$$u_k(\mathbf{x}',t') = \sum_{i=1}^{S} \int_{-\infty}^{\infty} \int_{V_0} g_{k,i}(\mathbf{x}',t';\mathbf{x},t) f_i(\mathbf{x},t) dx^3 dt, \tag{2.1}$$

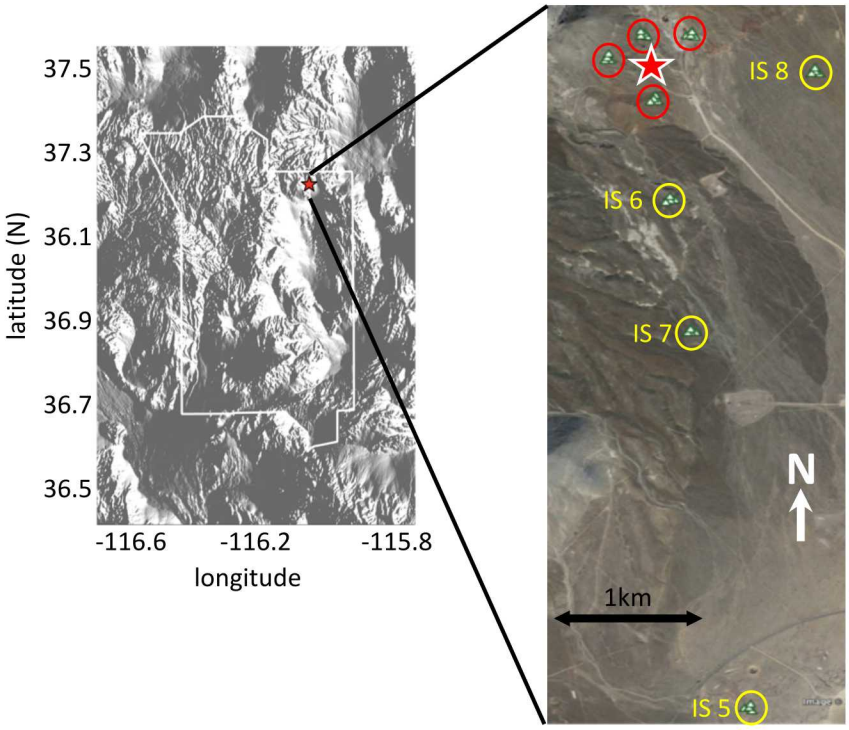


**Figure 2.1.** Location of SPE Phase 1. Left: Overview map showing the outline of the NNSS (in white), where the location of the experiment is shown by the red star. Right: Expanded view of the SPE Phase 1 area. The surface location of the explosions are shown by the red star and the infrasound stations are indicated by the yellow circles. The yellow numbers correspond to the arrays that we use in the analysis, with an example of the data shown in Figure 2.2. Each array, approximately 50m in aperture, contained four infrasound stations in a triangular shape, with a single station in the center and three stations at the corners. The red circles indicate the locations of the infrasound arrays that are not analyzed in this paper due to the superposition of the seismic and infrasonic first arrivals.

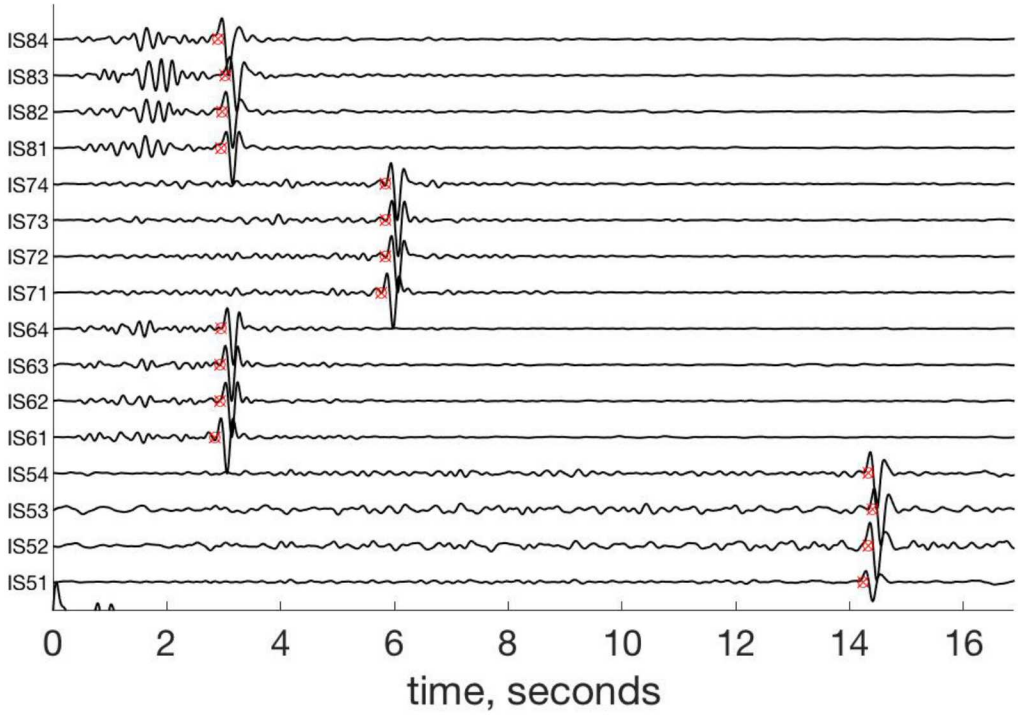


**Figure 2.2.** Acoustic data for SPE3, filtered to 1-6 passband and trace normalized. The red marks immediately prior to the largest arrival corresponds to the theoretical arrival of the first acoustic energy, assuming a sound speed of 343m/s and a straight-line propagation from the source location to the corresponding receiver. Note the prominent pre-acoustic arrivals for stations IS61-IS64 and IS81-IS84, which we interpret as seismic energy being recorded on the acoustic sensors. The station numbers correspond to the map locations indicated in Figure 2.1.

where $u_k$ is the displacement acoustogram, $g_{k,i}$ is the Green's function describing the impulse response from source $i$, of which there are $S$, located at $\mathbf{x}$ to receiver $k$ at $\mathbf{x}'$, $f_i$ is the sum of the equivalent body forces, and $V_0$ is the source volume which contains the non-zero portion of $f_i$ (Stump and Johnson, 1977). We explicitly assume that the source of the acoustic energy results from two mechanisms: 1) an explosion located underground and 2) explosion-generated spall, which is located at the Earth's surface directly above the explosion. Note that the actual explosion occurs underground, resulting in non-linear deformation of the Earth in the immediate vicinity of the explosion. However, this region is small relative to the scale of the source-receiver distance, so we make the simplification that the explosion results in purely elastic seismic waves radiating from a point. The assumption is that the seismic energy from the explosion converts to acoustic energy at the Earth's free surface via linear mode conversion. The second source term in our model attempts to simulate the spall of the Earth's surface directly above the explosion source. As with the explosion term, spall is highly non-linear, but over the scale of the source-receiver distance, the spall source is small enough to be approximated by a purely vertical, time-dependent force acting on the Earth's surface directly above the explosion source. Based on these simplifications, our forward model of the far-field acoustic energy is given as a convolution of the equivalent source with the atmospheric Green's function:

$$\begin{aligned} u_k(\mathbf{x}',t) &= \sum_{i=1}^{2} \Big( G_{k,i}(\mathbf{x}';\mathbf{x}_i,t) \otimes f_i(\mathbf{x}_i,t) \Big) \\ &= \Big( G_{1,k}(\mathbf{x}';\mathbf{x}_1,t) \otimes \mathbf{M}_{expl}(\mathbf{x}_1,t) \Big) + \Big( G_{2,k}(\mathbf{x}';\mathbf{x}_2,t) \otimes \mathbf{F}(\mathbf{x}_2,t) \Big) \\ &= G_{1,k}(\mathbf{x}';\mathbf{x}_1,t) \otimes \begin{bmatrix} M_{xx} & 0 & 0 \\ 0 & M_{yy} & \\ 0 & 0 & M_{zz} \end{bmatrix} + G_{2,k}(\mathbf{x}';\mathbf{x}_2,t) \otimes \begin{bmatrix} 0 \\ 0 \\ F_z \end{bmatrix} \end{aligned} \tag{2.2}$$

where $\otimes$ denotes time-domain convolution, $G_{1,k}(\mathbf{x}';\mathbf{x}_1,t)$ and $G_{2,k}(\mathbf{x}';\mathbf{x}_2,t)$ are the atmospheric Green's functions from the source located at $\mathbf{x}_1$ and $\mathbf{x}_2$, respectively, to the receiver $k$ located at $\mathbf{x}'$ for a time domain moment tensor $\mathbf{M}_{expl}$ and a surface-located time-dependent force $\mathbf{F}$, respectively. For our model, we explicitly assume that $\mathbf{M}_{expl}$ is an buried isotropic explosion, and thus $M_{xx} = M_{yy} = M_{zz}$. Likewise, we assume that the force term is purely in the vertical direction, which is the result of spall.

Rewriting equation 2.2 in the frequency domain yields

$$u_k(f) = \sum_{i=1}^{2} G_{k,i}(f) m_i(f) \tag{2.3}$$

where $m_1 = \mathbf{M}_{expl}(f)$ and $m_2 = \mathbf{F}(f)$ are the spectra of the source terms. In matrix form, equation 2.3 is written as

$$\mathbf{u} = \mathbf{G}\mathbf{m} \tag{2.4}$$

which allows us to solve for the spectra of each assumed source term. Writing out the terms in equation 2.4 yields

$$\begin{bmatrix} u_1(f_1) \\ u_1(f_2) \\ \vdots \\ u_1(f_N) \\ \\ u_2(f_1) \\ u_2(f_2) \\ \vdots \\ u_2(f_N) \\ \\ \vdots \\ \vdots \\ \\ u_K(f_1) \\ u_K(f_2) \\ \vdots \\ u_K(f_N) \end{bmatrix} = \begin{bmatrix} \mathbf{G}_{1,1} & \mathbf{G}_{1,2} \\ \mathbf{G}_{2,1} & \mathbf{G}_{2,2} \\ \mathbf{G}_{3,1} & \mathbf{G}_{3,2} \\ \vdots & \vdots \\ \mathbf{G}_{K,1} & \mathbf{G}_{K,2} \end{bmatrix} \begin{bmatrix} m_1(f_1) \\ m_1(f_2) \\ \vdots \\ m_1(f_N) \\ \\ m_2(f_1) \\ m_2(f_2) \\ \vdots \\ m_2(f_N) \end{bmatrix} \tag{2.5}$$

where $\mathbf{G}_{k,1}$ are the Green's functions for the isotropic moment term for stations 1-$K$, and $\mathbf{G}_{k,2}$ are the Green's functions for the vertical force term. The structure of $\mathbf{G}_{k,i}$ takes the form

$$\mathbf{G}_{k,i} = \begin{bmatrix} G_{k,i}(f_1) & \dots & 0 \\ \\ \vdots & \searrow & \vdots \\ \\ 0 & \dots & G_{k,i}(f_N) \end{bmatrix} \tag{2.6}$$

where $G_{k,i}(f_j)$ is the Green's function for source $i$ (for frequency index $j$) for the $k^{th}$ receiver station.

The system of equations shown in equations 2.5 can be solved in a least squares sense:

$$\mathbf{m} = \left(\mathbf{G}^{\dagger}\mathbf{G}\right)^{-1}\mathbf{G}^{\dagger}\mathbf{u} \tag{2.7}$$

where $[\cdot]^{\dagger}$ denotes the Hermitian transpose. We assemble the matrix equations 2.7 using the complex spectra of the raw acoustic data and the Fourier transformed Green's functions. We solve equations 2.7 by directly inverting the complex system, and the time dependent moment tensor components are obtained by inverse Fourier transforming the complex vector $\mathbf{m}$.

**Table 2.1.** SPE Phase 1 data analyzed in this report. DOB is depth-of-burial and SDOB is scaled depth-of-burial.

| **SPE event** | **Date of Experiment** | **Yield (tons)** | **DOB (m)** | **SDOB (m/kt$^{1/3}$)** |
|---|---|---|---|---|
| SPE-2 | 25 October, 2011 | 1.0 | 54.9 | 365 |
| SPE-3 | 24 July, 2012 | 0.9 | 45.8 | 389 |
| SPE-5 | 26 April, 2016 | 5.04 | 76.5 | 356 |
| SPE-6 | 12 October, 2016 | 2.2 | 31.4 | 191 |

# Chapter 3

# Atmospheric Models and Green's Function Estimation

### 3.0.1 Atmospheric Predictions

The atmospheric Green's function describes the impulse response of the atmosphere from a given source type located at $\mathbf{x}$ to an acoustic receiver at $\mathbf{x}'$. It is a function of air temperature, pressure, humidity, surface topography, and wind speed. Therefore, to obtain an accurate estimate of the Green's function, one must obtain atmospheric conditions for all spatial points within a given region at a specific time. However, this type of information is difficult to obtain, and thus for the work presented here we estimate, or predict, the state of the atmosphere using publicly available, regional atmospheric observations. We use these observations as input to the Weather Research and Forecasting (WRF) program which compiles and interpolates atmospheric data and combines them with local topography to construct a high resolution atmospheric model. WRF is a mesoscale numerical weather prediction system originally developed by the National Center for Atmospheric Research (NCAR), the National Oceanic and Atmospheric Administration, the Naval Research Laboratory, the University of Oklahoma, and the Federal Aviation Administration (Skamarock *et al.*, 2008). The output from WRF is an three-dimensional atmospheric model describing, among other things, the temperature, pressure, and wind velocity of all points within the model. In our case, WRF incorporates ground surface topography and historical atmospheric data to construct a model that predicts the state of the atmosphere at the time of a given SPE event. We use output from WRF to build a three dimensional model of acoustic velocity which we use to simulate the impulse response of the atmosphere at the time of the SPE event, which we describe in the next section.

For each of the SPE events that we analyze, we produce two types of atmospheric-state models. In the first case, we produce an average model, which we designate a 10-year average model, based on the historical data collected for the actual experiment date as well as the nine years preceding the actual experiment date. The data that we use represents the atmospheric state on the specific day-of-year (DOY) of the SPE event for a one-hour window centered at the actual time-of-day (TOD) of the actual SPE event. The historical data is that which corresponds to the same one-hour window, but for each of the nine preceding years. An outline of the steps used to generate the 10-year average model are as follows:

1. Define the geographic region of interest. Note that for this work, the region of interest is rectanglar, approximately 2000m wide in the east-west direction by 5500m in the north-south direction. The region is defined by the actual SPE event located at latitude 37.221207N and longitude 116.0608674W (Figure 2.1).

2. Obtain topography information corresponding to the same area defined in the previous step. For our work, we obtained topography data from http://viewer.nationalmap.gov/basic/. The resolution of this data is 1/3 arc second in both cardinal directions.

3. Gather weather data in the region of interest. For our work, we obtained data from the University Corporation for Atmospheric Research (UCAR) at rda.ucar.edu. We gathered a single day's worth of atmospheric data around the actual experiment time. We also gather data for the same day-of-year (DOY) for the nine years preceding the actual experiment date. We then cull the atmospheric data to include only a one hour window around the actual experiment time.

4. Determine the mean atmospheric state as a function of altitude by averaging the ten atmospheric states obtained in the previous step.

5. Build an atmospheric model for the region of interest. The topography information combined with the mean atmospheric state are used as input to WRF. WRF will use these data to predict the state of the atmosphere at the estimated (or actual) experiment time.

6. Estimate the Green's functions. The atmospheric model estimated by WRF is used as input to a finite difference scheme to estimate the impulse response of the atmosphere for each source type for all points in the model.

In addition to the 10-year average models, we also produce two extrema models for each SPE event, which are also based on the historical atmospheric data collected during the construction of the 10-year average models. Specifically, based on the ten predicted atmospheric states that we obtained in step 4 above, we choose two extrema states: for example, the DOY/TOD data that corresponds to the warmest and windiest conditions, or the coolest and calmest conditions. Each of these extrema models is constructed with data that corresponds to the DOY/TOD for a given SPE event, but can be from any one of the ten years prior to the actual SPE event: no averaging is performed in this case. We choose the extrema conditions in order to maximize the variability in acoustic wave speeds. Using the two extrema models, we then create additional Green's functions estimates. Therefore, for each SPE event, we produce six sets of Green's functions: two sets for each atmospheric model, where each set of Green's functions corresponds to a buried explosion source and a surface spall source.

The steps listed above outline a method of predicting the state of the atmosphere at the actual time of a given SPE event, and is based strictly on historical, regional-scale observations of the atmosphere. The resulting atmospheric models do not contain any data that is actually measured on-site at the time of the experiment, and thus we refer to these models as Atmospheric Predictions. In a subsequent SAND report, we will describe a method to incorporate atmospheric measurements

obtained locally, and at the actual time, of a given experiment. The eventual goal will be to compare the analysis results using predicted versus actual weather data.

For each SPE event, we show a summary of the atmospheric wind speed and temperature as a function of altitude (Figure 3.1 and Table 3.1). Note that, for example, the warmest-windiest year didn't necessarily exist for each SPE event. Rather, we chose a representative temperature/wind speed combination that generally produced the largest variability in acoustic wave speed for a given SPE event. Also, we eliminate from consideration any years that contained near-surface wind speeds greater than 5 m/s, as SPE explosions were not conducted in these conditions.

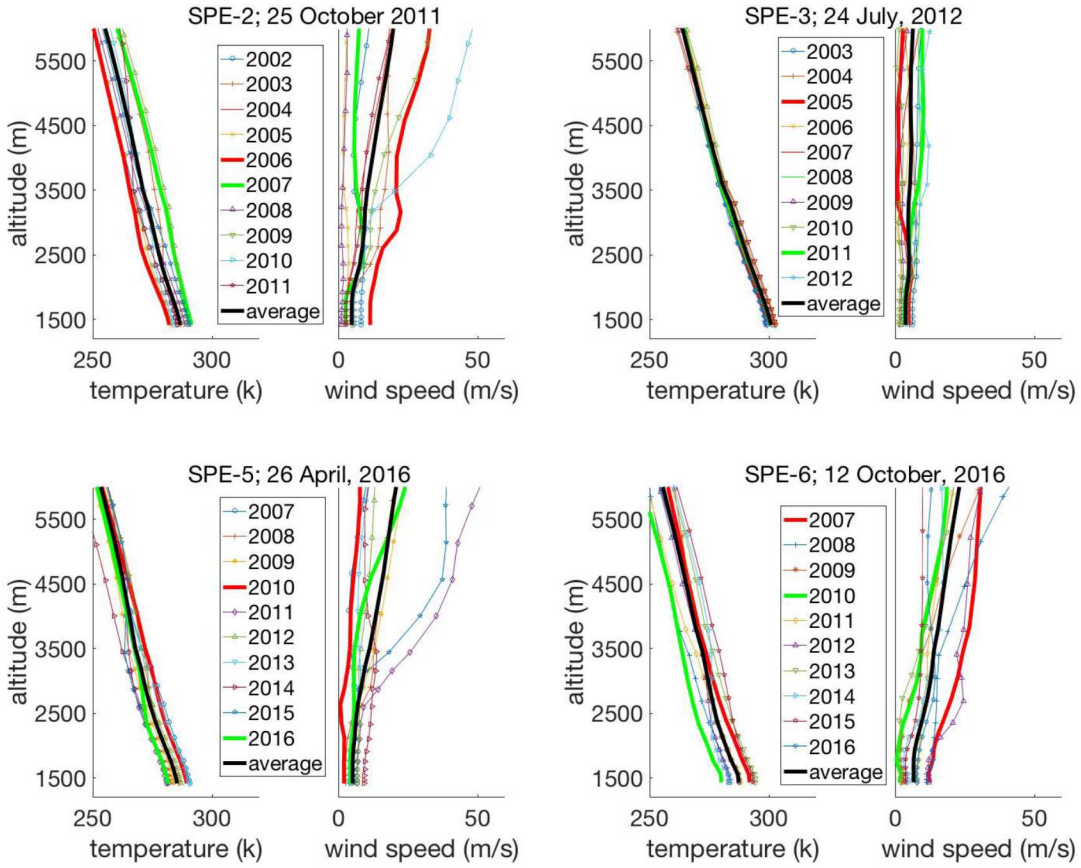


**Figure 3.1.** Atmospheric models produced by WRF based on ten years of regional meteorologic observations, for each of the SPE events that we analyzed. For each panel, we show the temperature and wind speed as a function of elevation above mean sea level, where the average model is indicated by the heavy black line and the extrema years are indicated by the heavy red and green lines (Table 3.1).

**Table 3.1.** Atmospheric extrema for a given day-of-year for the ten years preceding a given SPE event.

| SPE event | SPE date | first extrema combination | second extrema combination |
|---|---|---|---|
| SPE-2 | 25 October, 2011 | 2006; cool and windy | 2007; warm and calm |
| SPE-3 | 24 July, 2012 | 2005; warm and calm | 2011; cool and windy |
| SPE-5 | 26 April, 2016 | 2010; warm and calm | 2016; cool and windy |
| SPE-6 | 12 October, 2016 | 2006; warm and windy | 2009; cool and calm |

### 3.0.2 Green's Function Estimation

Recall that we model the infrasonic data as combination of two source phenomena: a buried explosion and surface spall. Therefore, for each atmospheric model we produce two sets of Green's functions. For the first set of Green's functions, we simulate an isotropic explosion located at a depth that corresponds to the given SPE event that we are analyzing. The Green's function resulting from the spall is modeled as a vertically oriented point force located on the Earth's surface directly above the explosion location. For each source type, we simulate the Green's functions using the SANDIA-developed code, TDAAPS, which is a staggered grid finite difference algorithm (Symons *et al.*, 2006). TDAAPS takes into account the surface topography of the SPE field area as well as the relevant atmospheric variables (wind speed, pressure, humidity, etc.) to solve the time domain velocity-pressure system of the acoustic wave equation. For each SPE event and atmospheric model, the two source terms are simulated as band-limited (35-360 Hz, at a 1% level) delta functions at the appropriate time and space, and the scheme propagates the wave field to all points in the model. The model contained 852, 2232, and 404 discrete nodes in the $x$, $y$, and $z$ directions, respectively, with a node size of 2.4m, and a time step of 0.0014 seconds. Based on these parameters and the acoustic velocity range in the models, the CFL stability criteria was $< 0.59$, minimizing the effects of numerical dispersion and/or artifacts in the calculation of the Green's functions. Finally, for regions of the model that are located beneath the Earth's surface, the scheme approximates the Earth as a fluid with a velocity of 500 m/s, which precludes the modeling of physically realistic seismic arrivals.

# Chapter 4

# Results

Prior to analysis, we upsample the observed acoustic data to the sample rate of the Green's functions. Although it would be more computationally efficient to down sample the Green's functions to that of the data (200Hz), we found that doing so introduced spurious, high frequency artifacts to the Green's functions that are likely associated with decimation. We then manually align the acoustic first arrivals of the Green's functions with those of the observed data, transform the data and Green's functions to the frequency domain via a forward Fourier transform, form the matrix equations, and invert the complex spectra directly. The inversion solves for the complex spectra of both source terms simultaneously, from which we obtained the time-domain source terms by applying the inverse Fourier transform. The final results were band passed to 1-5Hz, which corresponds to the frequency band of the infrasonic data (figure 4.1).

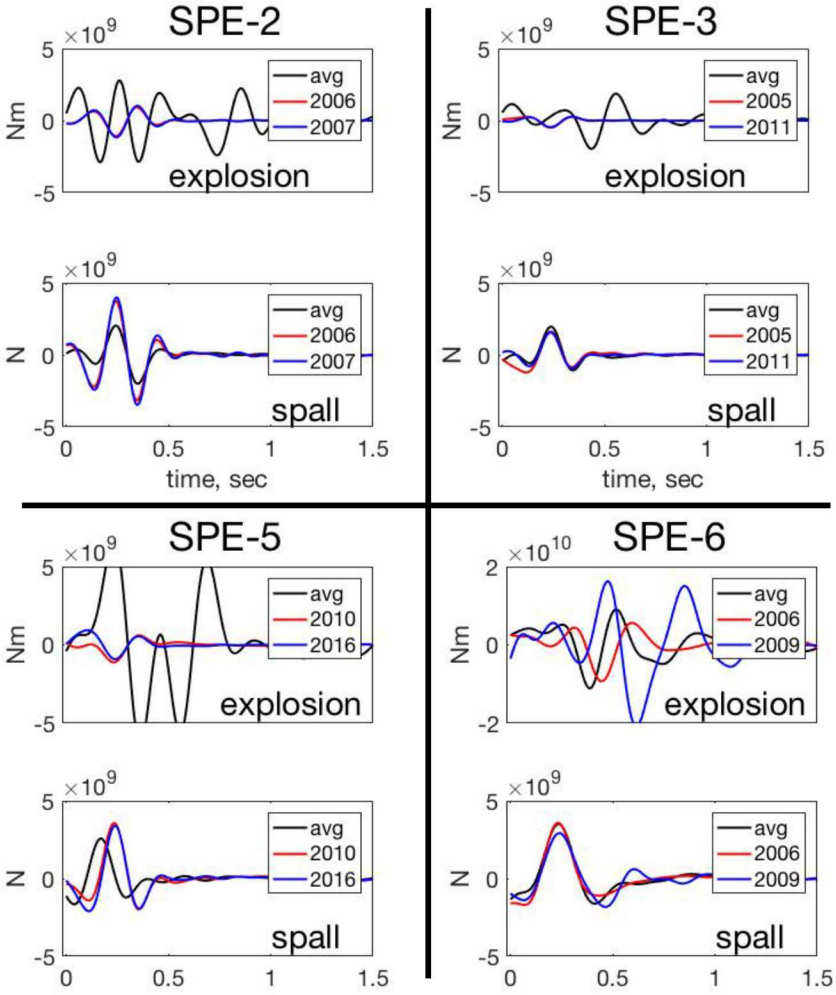


**Figure 4.1.** The inversion results, for each SPE event, band passed filtered to 1-5Hz. For each panel, we show the estimated time domain moment tensor terms for each presumed source mechanism: an isotropic explosion and the surface-located spall. The results obtained using the 10-year average atmospheric models are shown in black, and the results using the extrema models are shown in red and blue, according to the legend. Note that the results for the vertical force tensor term (i.e. spall) are quite stable and repeatable, whereas the results for the explosion term are not.

The most apparent result is that the explosion source term is highly erratic for a given SPE event, depending on the atmospheric model. Additionally, the estimated explosion source term is extremely variable from one SPE event to the next. Conversely, the estimated spall source term is remarkably similar for all four SPE events and from model to model. We summarize our observations as follows:

1. SPE-2: The estimated explosion source term for the 10-year average atmospheric model is quite erratic and different from the estimated explosion source terms for the extrema atmospheric models. However, the explosion source terms estimated using the two extrema models are quite similar to each other. For the estimated spall terms, the wave forms and timing are similar, with the major difference being the smaller amplitude of the spall term estimated using the 10-year average model.

2. SPE-3: The estimated explosion source terms for this SPE event behave similarly to those of the SPE-2 event: the explosion source term for the 10-year average model is significantly different than those estimated using the extrema atmospheric models. Also, the explosion source terms for both of the extrema models are virtually identical. The estimated spall terms are remarkably similar for all three atmospheric models for this SPE event.

3. SPE-5: The estimated explosion source terms for this SPE event behave similarly to those of the SPE-2 and SPE-3 events: the explosion source term for the 10-year average model is significantly different, and higher amplitude, than those estimated using the extrema atmospheric models. In addition. The spall terms estimated using the extrema atmospheric models are virtually identical. The spall term estimated using the 10-year average model has a similar waveform as those estimated using the extrema models, but is advanced in time.

4. SPE-6: The estimated explosion terms are different for all three atmospheric models, showing no obvious similarities from one model to the next. However, the estimated spall terms are similar for all three models.

5. For SPE 2,3, and 5, the estimated explosion terms are similar for the extrema models whereas the explosion term estimated using the 10-year average model is the outlier.

6. The relative amplitudes of the estimated spall terms don't appear to scale to the scaled depth-of-burial. If they did, we would expect the amplitude of these terms would all be roughly similar for SPE 2, 3, and 5 whereas the amplitude of the estimated spall term for SPE 6 would be roughly one-half that of the other three.

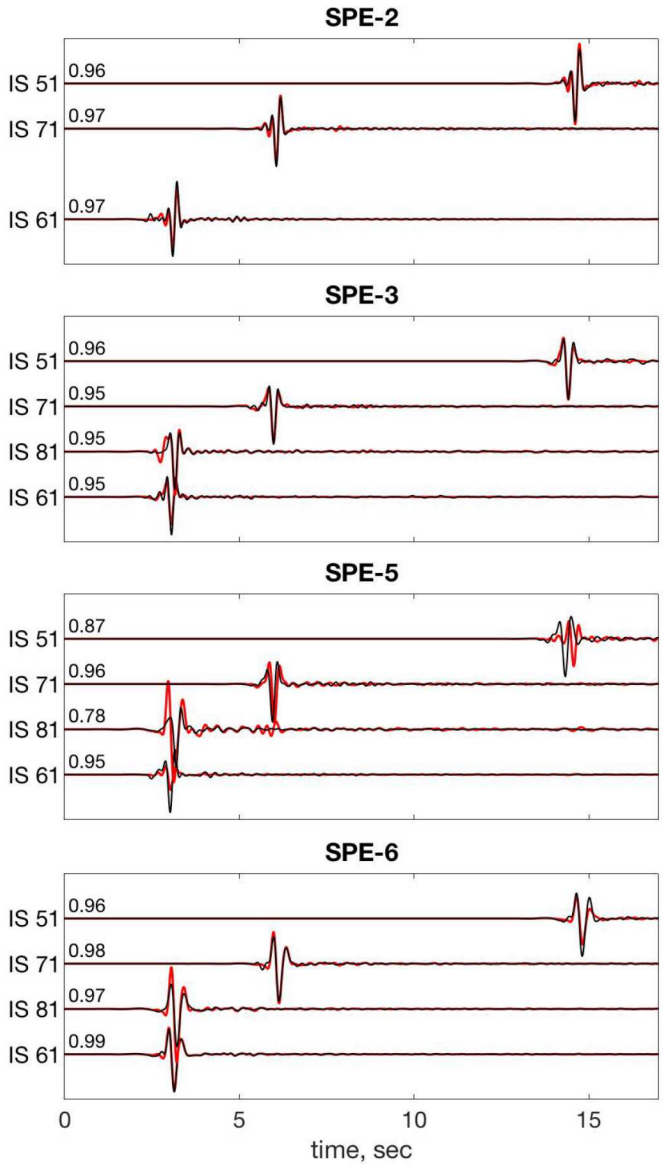


**Figure 4.2.** Comparison between the observed data (black) and the synthetic data predicted by convolving the estimated time domain moment tensor terms with the Green's functions estimated using the 10-year average atmospheric models (red). The correlation coefficients between the observed and synthetic data are marked above the traces. Note that the data for array IS8 was not available for SPE-2.

In general, the inversion results fit the data extremely well. To illustrate this, for each SPE event we convolved the estimated source terms with the corresponding Green's functions, and summed the resulting time series. These time series are referred to as computed data and represent the predicted data in equation 2.2. In figure 4.2 we show the predicted data plotted on top of the observed data, bandpass filtered to 1-5Hz, and their corresponding correlation coefficients. Because of space limitations, we only show one time series for each acoustic array and only for the 10-year average model. However, these results are typical, with the average correlation coefficient for all the data and all the models equal to 0.96. The data misfit for SPE-5 was the worst, which we attribute to this event having the largest explosive yield. In this case the linear assumptions made in our inversion we violated to the greatest degree as compared to the three other SPE events.

# Chapter 5

# Discussion

For this work, we have two primary goals: assess the effects of varying atmospheric models on the inversion of infrasonic data for the equivelent time domain moment tensor and determine the relative contribution of the moment tensor terms to the observed data. In general, the different atmospheric models have a greater effect on the estimated explosion term than the estimated spall term. Also, the estimated spall term is much more stable from model to model and from SPE event to SPE event. We suggest that these results are due to the fact that the spall term is the major contributor to the observed infrasonic data and thus are less effected by noise in the data or uncertainties in the estimates of the Green's functions.

Spatial and temporal changes in atmospheric temperature and wind speeds can have significant effects on the propagation of sound waves. Indeed, there is a rich literature on the effects of the atmosphere on regional scale (100s of km) infrasonic propagation (see McKisic, 1997, for an extensive review), where factors such as temperature and stratospheric winds significantly affect the detection and subsequent inversion of infrasound data. However, in this paper we focus on the variability of the atmosphere at the local scale (1-5km), where the infrasonic signals are confined to the lower troposphere. At these lower levels in the atmosphere, local effects such as a strong temperature gradient, local wind, topography, and convection are the dominant factors that effect sound propagation. Without taking any actual atmospheric measurements at the field site during a given SPE event, we relied on publicly available, regional scaled meteorologic observations to estimate the physical state of the atmosphere for each SPE event. The question we attempt to resolve here is whether this approach can be used in the inversion process to yield stable and accurate estimates of the seismo-acoustic source.

Ultimately, the atmospheric model used to estimate the Green's functions will affect the arrival time of the acoustic arrival as well as the waveform of the impulse response. This is apparent in Figure 5.1 which shows, that for a given SPE event, differences in the arrival time of the (filtered) first arrival as well as the actual (filtered) waveform shape. This is more apparent on the farthest stations, as the longest travel distance will lead to the longest ray path increasing the number of times a given ray is influenced by the atmosphere. We mitigate the effects of acoustic arrival time differences by manually lining up the acoustic arrivals of the Green's functions with those observed in the data. This accounts for errors in the Green's functions based on incorrect assumptions of the atmospheric sound speed, but does not account for errors of the Green's function's wave form. Therefore, differences in the inversion results are likely solely due to the differences in the waveform of the Green's functions rather than differences between observed and predicted acoustic

arrival times.

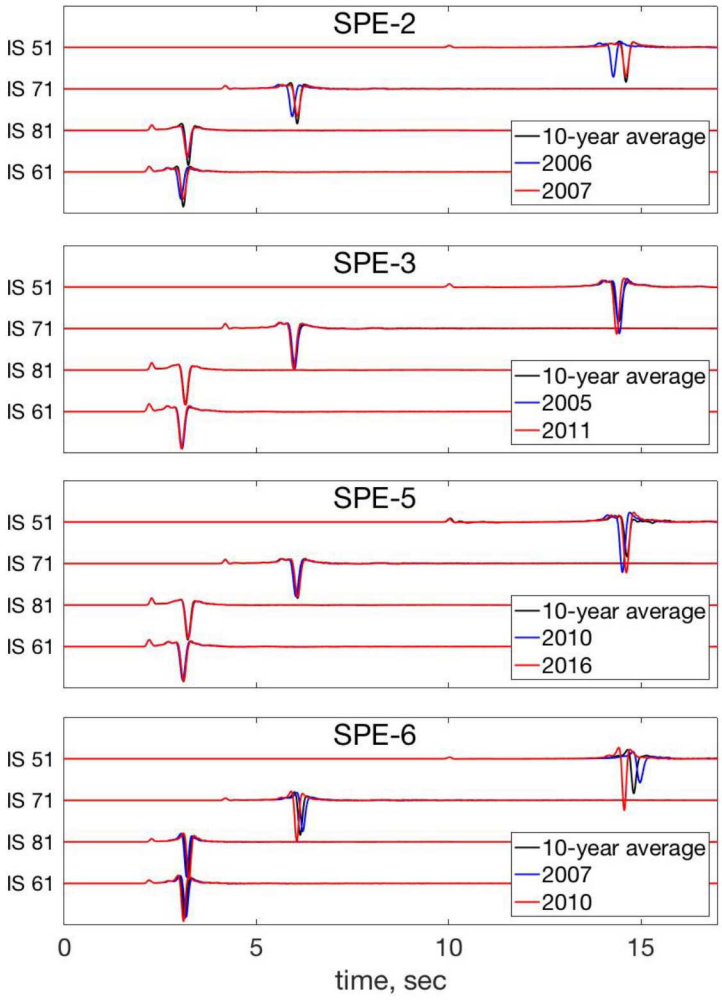


**Figure 5.1.** Estimated spall Green's functions for the three atmospheric models, for four SPE events. The Green's functions are convolved with a Gaussian (center frequency of 10Hz) for display purposes, and we only plot the Green's functions for the first station of each array (stations IS51, IS61, IS71, and IS81), in order of increasing radial distance from the source. For each SPE event and each station, we plot the three Green's functions, one for each atmospheric model, that corresponds to the 10-year average model (black), and the two extrema models (blue and red). For each station, the Green's function is normalized to the maximum amplitude of the Green's function estimated using the 10-year average atmospheric model.

Recall that we assume that there are two sources of infrasonic energy: the buried explosion and the surface spall. Our results show that for each SPE event, the estimated spall term is highly repeatable whereas the estimated explosion term is not. If both of the actual source terms were equal contributors to the data, we'd expect to see that both of the estimated source terms to be equally affected by the differences in the Green's functions, which is not the case. We interpret this as being the result of two reasons. First, the largest contributor to the infrasonic signal is the non-linear upheaval of the ground (spall), producing a momentary overpressure in the atmosphere. Although the spall is confined to a relatively small area of the ground surface (radius of 10s of meters) directly above the explosion, it has a vertical displacement amplitude of several centimeters to meters. This is in contrast to the linear coupling of seismic energy energy into infrasonic energy, which occurs over a much larger area but with displacement amplitudes that are several orders of magnitudes lower than those associated with the spall. In this scenario, the relative contribution of the spall source term dominates the data. This explanation of the infrasonic signal generation is supported by the similarity of infrasonic data from SPE-2 and SPE-3 to synthetic infrasound data modeled by the Rayleigh integral (Jones *et al.*, 2015; Whitaker, R., 2007, 2008, 2009). In these simulations, it was found that the data could be accurately explained by a single spall term, with no need for a contribution from a buried explosion term.

If the data contains very little actual contribution from the explosion source term, then the explosion source term occupies the null space of the inversion: the estimated explosion source terms are virtually uninformed by the data, meaning that they can vary greatly without any significant obligation to fitting the data. The large degree of variation in the estimated explosion source term is likely due to noise in the data or errors in the estimated explosion Green's functions, which would have a relatively much larger effect on this model parameter (Stump, 1977). To test this assertion we invert the data for three different scenarios, corresponding to three different assumed source mechanisms. Specifically, using the Green's functions for the 10-year average atmospheric model, we parameterize the inversion using only the spall term, only the explosion term, and then both of the source terms. We then invert the data for all four SPE events, and compute the average correlation coefficient (Table 5.1). To compute the average correlation coefficients, we convolve the Green's functions for each station with the time-domain moment tensors estimated by the inversions (equation 2.2), filter to a passband of 1-5Hz and correlate the resulting time series with the observed data, also passband filtered to 1-5Hz. We then average all the resulting correlation coefficients for each station for each case. In all cases, when the data is inverted using only an explosion source term the average correlation coefficient is much lower, with a greater degree of variability, than when we invert the data using a spall Green's function (Figure 5.2). This result corroborates earlier works (e.g. Jones *et al.*, 2015; Whittaker, 2007, 2008, 2009) which claimed that the dominant source of infrasound signal at SPE 2 and 3 is from surface spall rather than the linear elastic-to-acoustic coupling at the Earth's surface.

The second contributing factor to the instability of the estimated explosion source term may be that our forward model does not adequately simulate the seismic energy generated from the buried source. Specifically, the seismic wave field generated from a buried explosion is fully elastic, and will generate significant Rayleigh waves. In addition to the direct conversion of P-wave energy to acoustic energy, the propagation of surface waves will also generate a infrasonic signal (Che *et al.*, 2014). However, our method of modeling the acoustic Green's functions does not simulate

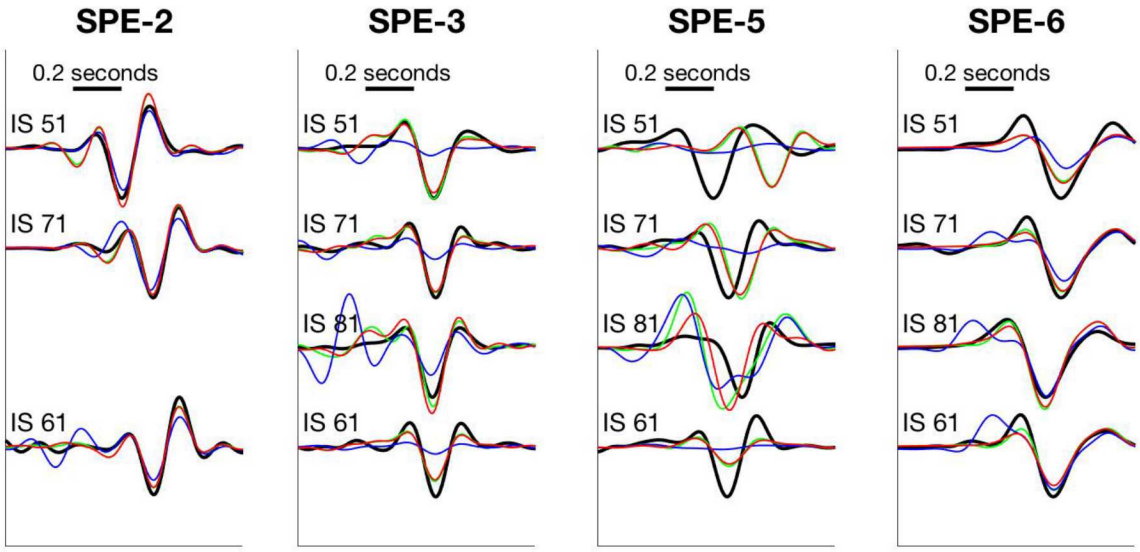


**Figure 5.2.** Data misfits for different source models. We show the observed data (black) for the first station from each array, for all four SPE events that we analyze. Note that we window the data about the approximate first acoustic arrival for clarity. The green, red, and blue correspond to synthetic data where the assumed model is parameterized by both a spall and explosion term, a spall term only, and an explosion term only, repectively. To compute the synthetic data, we convolve the estimated source term with the relevant Green's function (see text). Note the high degree of data misfit when the inversion is parameterized by only an explosion term (blue curves).

**Table 5.1.** The data misfit for three scenarios, for each SPE event and atmospheric model.

| SPE event | atmos. model | expl. only | spall only | expl+spall |
|---|---|---|---|---|
| SPE-2 | 10-year | 0.89±0.10 | 0.95±0.01 | 0.96±0.01 |
| | 2006 | 0.79±0.11 | 0.97±0.01 | 0.92±0.04 |
| | 2007 | 0.76±0.13 | 0.97±0.02 | 0.91±0.02 |
| SPE-3 | 10-year | 0.73±0.11 | 0.94±0.03 | 0.94±0.03 |
| | 2005 | 0.74±0.11 | 0.96±0.02 | 0.96±0.03 |
| | 2011 | 0.78±0.14 | 0.97±0.01 | 0.93±0.04 |
| SPE-5 | 10-year | 0.71±0.09 | 0.92±0.06 | 0.91±0.05 |
| | 2010 | 0.75±0.12 | 0.93±0.07 | 0.93±0.07 |
| | 2016 | 0.75±0.12 | 0.93±0.07 | 0.92±0.07 |
| SPE-6 | 10-year | 0.89±0.09 | 0.96±0.02 | 0.98±0.01 |
| | 2006 | 0.77±0.14 | 0.95±0.02 | 0.98±0.01 |
| | 2009 | 0.92±0.05 | 0.97±0.01 | 0.98±0.01 |

elastic or Rayleigh waves. Rather, it treats the Earth as a fluid with a sound speed of 500 m/s, which precludes simulation of linear *P*-to-acoustic and Rayleigh-to-acoustic coupling. We view this as major limitation of this work, which we will address in a future work where we couple the elastic region of the model to an acoustic model. This combined model can then be used to more accurately estimate the acoustic Green's function resulting from the buried explosion source.

# Chapter 6

# Conclusions

We inverted the infrasonic data from four SPE experiments for the linear-equivalent seismo-acoustic time-domain moment tensor, assuming that the combined source consisted of a linear combination of a buried isotropic explosion and surface spall. To estimate the atmospheric forward models, we combined region-scaled atmospheric observations with the local topography to construct a series of models from which we estimated the atmospheric Green's functions. All of the models were based on atmospheric observations that corresponded to the day-of-year and time-of-day of the actual SPE events. For each SPE experiment, we constructed Green's functions for three atmospheric states: one based on an average of ten SPE-specific DOY/TOD observations and two extrema models that were chosen to maximize the variability in the acoustic wave speed.

We parameterized the inversion with two assumed source terms: a buried isotropic explosion and surface spall. The results of the inversion showed that the estimated spall term is relatively stable and repeatable for all of the SPE data that we invert, regardless of the atmospheric model that we used. Conversely, the estimated explosion term is highly variable in all cases. When we invert the data for only a spall term, the results are also stable and repeatable with a very low degree of data misfit. This suggests that the explosion term is not a significant contributor to the observed infrasonic data and/or our model of the elastic-to-acoustic linear mode conversions is too simplistic.

To test whether the buried, isotropic explosion term is an actual contributor to the observed data, it is necessary to more accurately simulate the elastic-to-acoustic mode conversions. Specifically, our inversion simulated the Earth as a fluid with a high acoustic velocity, which precluded the simulation of actual elastic energy. Seismic wave fields are known to contribute to infrasonic energy via linear body wave to acoustic and Rayleigh to acoustic mode conversions. We will address these phenomena in future work.

The high degree of repeatability of the estimated spall terms, regardless of the assumed source model, suggests that using regional-scale atmospheric observations to estimate the atmospheric Green's functions is a viable alternative to actual atmospheric measurements, which may not be available. However, to more thoroughly test this assertion, it is necessary to test our results with those obtained using actual atmospheric measurements, as well as an accurate model simulating all of the relevant phenomena of wave propagation.

# Chapter 7

# Acknowledgements

The authors also acknowledge the National Nuclear Security Administration, Defense Nuclear Nonproliferation Research and Development (DNN R&D), and the Source Physics Experiment (SPE) working group, a multi-institutional and interdisciplinary group of scientists and engineers. Sandia National Laboratories is a multimission laboratory managed and operated by National Technology and Engineering Solutions of Sandia LLC, a wholly owned subsidiary of Honeywell International Inc. for the U.S. Department of Energy's National Nuclear Security Administration under contract DE-NA0003525.

# Chapter 8

# References


Arrowsmith, S.J., J.B. Johnson, D.P. Drob, and M.A.H. Hedlin (2010), The seismoacoustic wavefield: A new paradigm in studying geophysical phenomena, *Rev. Geophys.* **48**, doi:10.1029/2010RG000335.

Che, I-Y, J. Park, I Kim, T. S. Kim, H-I Lee (2014). Infrasound signals from the underground nuclear explosions of North-Korea, *Geophys. J. Int.* **198**(1), 495-505. doi: 10.1093/gji/ggu150.

Ford, S.R., A.J. Rodgers, H. Xu, D.C. Templeton, P. Harben, W. Foxall, and R.E. Reinke (2014), Partitioning of Seismoacoustic Energy and Estimation of Yield and Height-of-Burst/Depth-of-Burial for Near-Surface Explosions, *Bull. Seis. Soc. Am.* **104**(2), 608-623, doi: 10.1785/0120130130.

Gitterman, Y., Z. Ben-Avraham, and A. Ginzburg (1998). Spectral analysis of underwater explosions in the Dead Sea, *Geophys. J. Int.* **134**, 460-472.

Jones, K.R., R.W. Whitaker, S.J. Arrowsmith (2015). Modelling infrasound signal generation from two underground explosions at the Source Physics Experiment using the Rayleigh integral, *Geophys. J. Int.* **200**, 779-790. doi: 10.1093/gji/ggu443.

Patton, H.J., J.L. Bonner, and N. Gupta (2005). *Rg* excitation by underground explosions: insights from source modeling the 1997 Kazakhstan depth-of-burial experiment, *Geophys. J. Int.* **163**, 1006-1024.

Skamarock, W.C., J.B. Klemp, J.Dudhia, D.O. Gill, D.M. Barker, M. Duda, X. -Y. Haung, W. Wand, J.G. Powers (2008). A Description of the Advanced Research WRF Version 3, *National Center for Atmospheric Research*, Available at: http://www.mmm.ucar.edu/wrf/users/docs/arw_v3.pdf.

Snelson, C.M., R.E. Abbot, S.T. Broome, R.J. Mellors, H.J. Patton, A. J. Sussman, M.J Townsend, W.R. Walter (2013). Chemical Explosion Experiments to Improve Nuclear Test Monitoring, *EOS, Tans. Am. Geophys. Un.*, **94**(27), 237-239.

Stein, S., and M. Wysession, 2003, An Introduction to Seismology, Earthquakes, and Earth Structure, Blackwell Publishing, LTD., Malden, MA.

Stump, B.W and L.R. Johnson (1977). The determination of source properties by the linear

inversion of seismograms, *Bull. Seis. Soc. Am.* **67**, 1489-1502.

Stump, B.W., D.C. Pearson, and R.E. Reinke (1999). Source comparisons between nuclear and chemical explosions detonated at Rainier Mesa, Nevada Test Site, *Bull. Seis. Soc. Am.* **89**, 409-422.

Symons, N.P., D.F. Aldridge, D.H. Marlin, S.L. Collier, D.K. Wilson, V.E. Ostahsev (2006). Staggered-Grid Finite-Difference Acoustic Modeling with Time-Domain Atmospheric Propagation Suite (TDAAPS): Technical Report SAND2006-2540, Sandia National Laboratories.

Whitaker, R., 2007. Infrasound signals as basis for event discriminants, in *Proceedings of the 29th Monitoring Research Review: Ground-Based Nuclear Explosion Monitoring Technologies*, LA-UR-07-5613, Vol. 1, pp. 905-913, Available at:
http://www.osti.gov.bridge/product.biblio.jsp?osti_id=1027449.

Whitaker, R., 2007. Infrasound signals as basis for event discriminants, in *Proceedings of the 30th Monitoring Research Review: Ground-Based Nuclear Explosion Monitoring Technologies*, LA-UR-08-05261, Vol. 1, pp. 912-920, Available at:
http://www.osti.gov.bridge/product.biblio.jsp?osti_id=960561.

Whitaker, R., 2007. Infrasound signals as basis for event discriminants, in *Proceedings of the 30th Monitoring Research Review: Ground-Based Nuclear Explosion Monitoring Technologies*, LA-UR-09-05276, Vol. 1, pp. 750-758, Available at:
http://www.osti.gov.bridge/product.biblio.jsp?osti_id=992203.

Yang, X. and J.L. Bonner (2009). Characteristics of Chemical Explosive Sources from Time-Dependent Moment Tensors, *Bull. Seis. Soc. Am.* **99**(1), 36-51, doi: 10.1785/0120080243.

# DISTRIBUTION:

| | | |
|---|---|---|
| 1 | MS MS0750 | Christian Poppeliers, 8861 |
| 1 | MS MS0750 | Katherine Anderson Aur, 6363 |
| 1 | MS MS0750 | Leiph Preston, 8861 |
| 1 | MS MS0750 | Steven R Vigil, 8861 |
| 1 | MS MS0899 | Technical Library, 9536 (electronic copy) |
| 1 | MS 0899 | Technical Library, 9536 (electronic copy) |


Sandia National Laboratories